

# On the Accuracy of RANS Simulations of 2D Boundary Layers with OpenFOAM

Sebastian Gomez<sup>1</sup>, Benjamin J. Graves<sup>2</sup>, Svetlana V. Poroseva<sup>3</sup>  
*University of New Mexico, Albuquerque, New Mexico, 87131*

OpenFOAM is an attractive Computational Fluid Dynamics solver for evaluating new turbulence models due to the open-source nature and the suite of existing standard model implementations. Before interpreting results obtained with a new turbulence model, a baseline for performance of the OpenFOAM solver and existing models is required. In the current study, we assess the accuracy of simulation results obtained with standard models for the Reynolds-averaged Navier-Stokes equations implemented in the OpenFOAM incompressible solver. Two planar (two-dimensional mean flow) benchmark cases generated by the AIAA turbulence Model Benchmarking Working Group are considered: the boundary layer on a zero-pressure-gradient flat plate and a bump-in-channel flow. OpenFOAM results are compared with the NASA CFD codes CFL3D and FUN3D. Sensitivity of simulation results to the grid refinement, linear pressure solvers, compressibility effects, and model implementation are analyzed. Testing is conducted using standard Spalart-Allmaras one-equation, Wilcox's 2006 version of the two-equation  $k-\omega$ , and SST 1994 turbulence models. Simulations using wall-resolved (low Reynolds number) formulations are considered.

## Nomenclature

$a_\infty$	=	Sonic velocity of air
$\tau_w$	=	Wall shear stress
$\rho$	=	Fluid density
$u$	=	Velocity fluctuation
$U$	=	Mean flow velocity
$U_\infty$	=	Free stream velocity
$C_f$	=	Skin friction coefficient, $\tau_w / \frac{1}{2} U_\infty^2 \rho$
$f_{v1}$	=	Empirical blending function; SA model
$N$	=	Total number of nodes in the computational domain
$h$	=	Characteristic mesh length for the constant domain size, $1/\sqrt{N}$
$k$	=	Turbulent kinetic energy
$L$	=	Characteristic length
$M$	=	Mach number
$Re_L$	=	Reynolds number based on $L$ , $U_\infty L / \nu$
$x$	=	Streamwise flow direction
$y$	=	Flow direction normal to a wall
$\nu$	=	Kinematic viscosity
$\varepsilon$	=	Dissipation rate of the turbulent kinetic energy
$\mu_t$	=	Dynamic turbulent viscosity of a fluid
$\nu_t$	=	Kinematic turbulent viscosity of a fluid, $\mu_t / \rho$
$\tilde{\nu}$	=	Spalart-Allmaras variable; SA model
$\omega$	=	Specific dissipation rate, $\varepsilon / k$

---

<sup>1</sup> Graduate Student, Mechanical Engineering, MSC01 1105, 1 UNM Albuquerque, NM, 87131-00011, AIAA Student Member

<sup>2</sup> Graduate Student, Mechanical Engineering, MSC01 1105, 1 UNM Albuquerque, NM, 87131-00011, AIAA Student Member

<sup>3</sup> Associate Professor, Mechanical Engineering, MSC01 1105, 1 UNM Albuquerque, NM, 87131-00011, AIAA Associate Fellow

## I. Introduction

Reliable and accurate modeling of wall-bounded turbulent flows is critical for most engineering applications. Direct numerical simulations (DNS) of the Navier-Stokes equations can accurately describe the turbulent flow characteristics. However, existing computational capabilities only allow DNS at Reynolds numbers much smaller than those pertinent to engineering applications. Therefore, a traditional approach to turbulence modeling at high Reynolds numbers is by solving modeled Reynolds-averaged Navier-Stokes (RANS) equations derived from the Navier-Stokes equations.

Commercial Computational Fluid Dynamics (CFD) codes provide a user with a list of RANS models to choose from. Commercial codes are convenient tools for engineering purposes, but they are not suitable for the verification and validation of new models. The open-source nature of OpenFOAM software<sup>1</sup> enables the implementation of new turbulence models into the existing library that already contains a few standard RANS models.

Before testing new models, the accuracy and reliability of simulation results obtained with the standard RANS models implemented in OpenFOAM should be established. This is the main goal of our current research. Three standard turbulence models are chosen for the task: Spalart-Allmaras (SA) model<sup>2</sup>, Wilcox's 2006 version of the  $k-\omega$  model<sup>3</sup>, and the Menter's version of Shear Stress Transport (SST) model<sup>4</sup>. Simulations were also conducted with the Isotropization-of-Production model by Launder, Reece, and Rodi<sup>5</sup> (LRR-IP) to test its capability in wall-bounded flows. The list includes one- and two-equation models as well as the Reynolds stress transport (RST) model.

The models' verification is conducted for two benchmark cases, namely, the boundary layer on a flat plate with the zero-pressure gradient (ZPG) and a flow over a bump in a channel. Both flows are incompressible planar (two-dimensional mean velocity field) flows. The cases were generated by the AIAA Turbulence Model Benchmarking Working Group<sup>6</sup>. A simplified version of the experimental geometry for the bump-in-channel flow, that is, without the suction slot, is used in the simulations. A sensitivity study is performed to analyze the grid resolution effect on the simulation results. The impact of using the incompressible OpenFOAM solver versus the compressible OpenFOAM solver at low Mach numbers and that of using different linear pressure solvers in OpenFOAM are also studied.

Results obtained with OpenFOAM are compared with those produced with the high-accuracy NASA codes CFL3D and FUN3D<sup>6</sup>.

## II. Numerical Simulations

### A. Computational Domains

The computational domain for the flat plate was  $2.33 \times 1$  units in the  $x$ - and  $y$ -directions. The flat plate wall boundary starts at  $x = 0$  and ends at  $x = 2$ . The plate is positioned at  $y = 0$ . The top of the computational domain is located at  $y = 1$ . The symmetry boundary condition is applied at  $x < 0$ . The no-slip boundary condition is used on the plate surface. At  $y = 1$ , zero gradients are assigned as the boundary condition for all variables.

The computational domain for a flow over a two-dimensional bump in a channel flow measures  $51.5 \times 5$  units in the  $x$ - and  $y$ -directions. The wall boundary starts at location  $x = 0$  and  $y = 0$ . The bump starts at approximately  $x = 0.4$ , and  $y = 0$ . The top of the bump is at  $x = 0.75$  and  $y = 0.05$ . The bump is symmetrical. The wall downstream of the bump ends at  $x = 1.5$ . The boundary conditions at the bottom of the computational domain at  $x < 0$  and  $x > 1.5$  are symmetry planes. The no-slip boundary condition is used on the wall. At the top of the computational domain, a symmetry plane is assigned as the boundary condition for all variables.

In the current research, structured grids generated at NASA<sup>6</sup> are used to avoid uncertainties associated with the grid generation process. The grids used for the flat plate have vertex dimensions of  $35 \times 25$ ,  $69 \times 49$ ,  $137 \times 97$ ,  $273 \times 193$ , and  $545 \times 385$  in the  $x$ - and  $y$ -directions, respectively. The grids for the bump-in-channel flow have vertex dimensions of  $89 \times 41$ ,  $177 \times 81$ ,  $353 \times 161$ ,  $705 \times 321$ , and  $1409 \times 641$  in the  $x$ - and  $y$ -directions, respectively.

### B. Turbulence Models

Model formulations and values of the model coefficients used in the current research were set to be in complete agreement with those provided by NASA<sup>6</sup>. To achieve this agreement, the models originally implemented in OpenFOAM had to be modified, as they *did not match the standard formulations* implemented in the NASA codes for the benchmark cases.

The SA turbulence model<sup>2</sup> is a one-equation RANS eddy viscosity model. Equations are solved for the mean velocity and an eddy-viscosity-like variable. The Wilcox 2006  $k-\omega$  model<sup>3</sup> is another two-equation model that solves transport equations for the turbulent kinetic energy,  $k$ , and the specific dissipation rate,  $\omega$ . The SST model<sup>4</sup> is also a two-equation model that solves transport equations for the turbulent kinetic energy and the specific dissipation rate

in the near wall region, while solving the transport equation for the dissipation rate,  $\varepsilon$ , in the free stream. The two areas are combined using a blending function developed by Menter<sup>4</sup>.

### C. Numerical Methods

The OpenFOAM solvers used in the current study are simpleFoam and rhoSimpleFoam. Both solvers utilize the Semi-Implicit Method for Pressure Linked Equations (SIMPLE) algorithm, but solve incompressible and compressible transport equations, respectively. The equations are discretized using the Gaussian integration scheme where values are interpolated from cell to face centers. The second-order Gauss scheme is used for every term in momentum and turbulence model equations. The central difference interpolation is used for all gradient terms. Upwind differencing is used for convective terms in all equations, but the scheme's order of accuracy varies for the momentum and turbulent transport equations: the second-order scheme is applied to the terms in the momentum equations and the first-order scheme is used in the turbulent transport equations. It was found that using the second-order scheme for variables in the turbulent transport equations led to underestimating the turbulent kinetic energy prior to the freestream region comparing to the NASA data. Changing the scheme's accuracy to the first order led to better agreement between OpenFOAM and NASA's results.

In OpenFOAM, second- and first- order schemes are referred to as linearUpwind, and upwind, respectively. The central difference interpolation scheme is used for the diffusion coefficient in all diffusive terms, and an explicit second-order non-orthogonal correction method is employed for surface-normal gradients. In OpenFOAM, these schemes are referred to as linear and corrected, respectively. More detail on numerical schemes implemented in OpenFOAM can be found in the OpenFOAM manual<sup>1</sup>.

## III. Results

### A. Flat Plate

In simulations, initial conditions for all flow variables correspond to the freestream values calculated for the boundary conditions. The pressure value of 1 atm is prescribed to the outlet and the internal field. The velocity boundary conditions at the inlet correspond to Mach number of 0.2, Reynolds number (based on  $L=1$ ) of 5 million with the reference temperature of 540 °R, which lead to the freestream velocity of 69.26 m/s .

In the SA model, the turbulence effects are described by the transport equation for the parameter  $\tilde{\nu}$ , which relates to  $\mu_t$  as  $\mu_t = \rho \tilde{\nu} f_{v1}$ , with  $f_{v1}$  being an empirical function<sup>2</sup>. In the current simulations of a flow over a flat plate, the boundary condition values for  $\tilde{\nu}$  are:  $\tilde{\nu}_{farfield} = 3\nu = 4.16 \times 10^{-5} \text{ m}^2/\text{s}$  and  $\tilde{\nu}_{wall} = 0$ . For the SST and  $k-\omega$  turbulence models, the boundary conditions for the freestream turbulent kinetic energy and the specific turbulence dissipation rate in the same flow are

$$k_{farfield} = 9 \times 10^{-9} a_\infty^2 \left( \text{here} = 1.125 \frac{U_\infty^2}{Re_L} \right) = 1.08 \times 10^{-3} \text{ m}^2/\text{s}^2$$

$$\omega_{farfield} = 1 \times 10^{-6} \frac{\rho_\infty a_\infty^2}{\mu_\infty} \left( \text{here} = 125 \frac{U_\infty}{L} \right) = 8.66 \times 10^3 \text{ s}^{-1}.$$

At the wall, the values of these parameters are:

$$k_{wall} = 0,$$

$$\omega_{wall} = 10 \frac{6\nu}{\beta_1(\Delta d_1)^2} = 4.35 \times 10^{10} \text{ s}^{-1}.$$

Initial and boundary conditions used in the current study for the SA, SST, and  $k-\omega$  turbulence models match those in Ref. 6.

In Figures 1-3, the results of simulations of a flow over a flat plate obtained on the 545x385 grid with the SA, SST, and  $k-\omega$  models are shown. They are presented at locations for which the NASA data is available. Profiles obtained with the SA model are shown in Fig. 1. Figures 2 and 3 show results obtained with the SST and  $k-\omega$  models, respectively. As the figures demonstrate, the agreement between the OpenFOAM results and those obtained with NASA's codes is good for all three models.

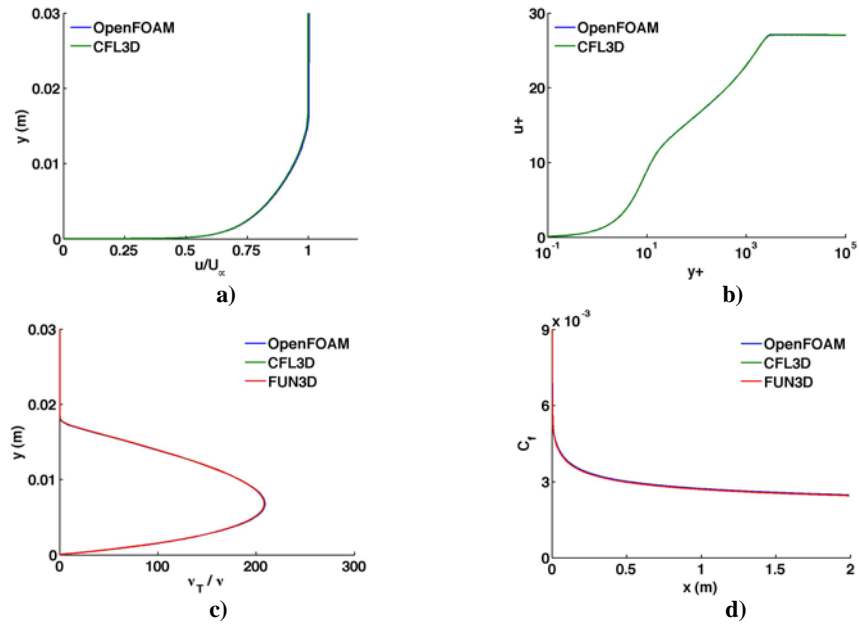


Figure 1. Results of the ZPG flat plate flow simulations with the Spalart-Allmaras turbulence model: a) mean velocity profile, b)  $U_+$ -profile, c)  $v_\tau$  at  $x = 0.97$  and d) skin friction coefficient.

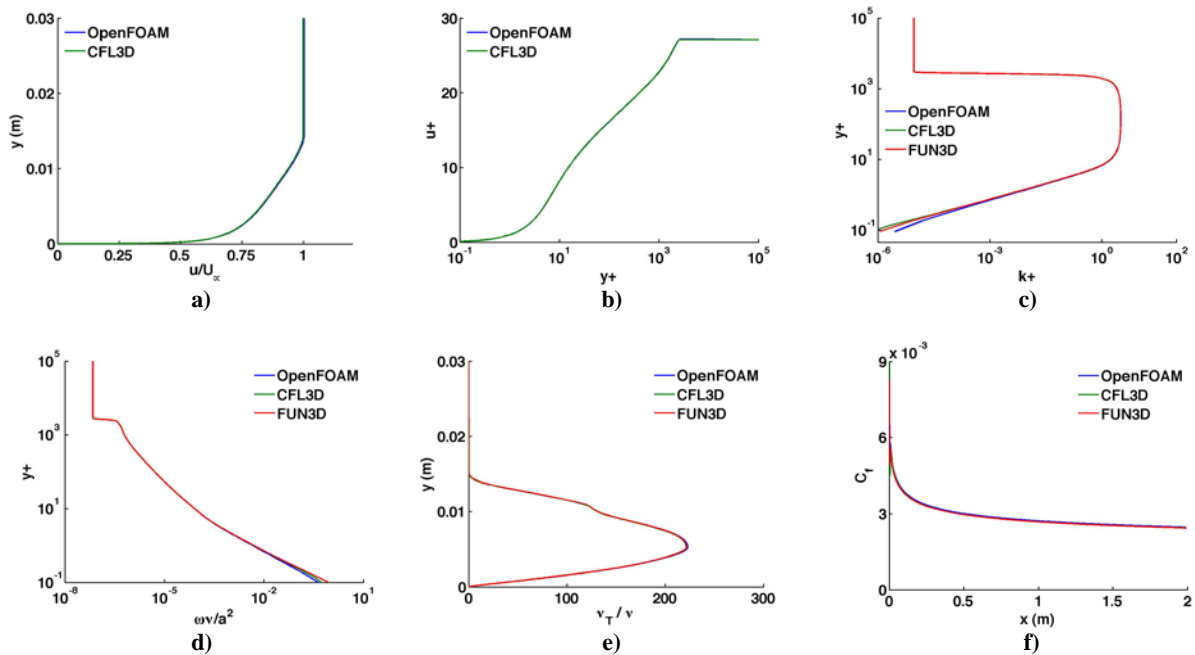


Figure 2. Results of the ZPG flat plate flow simulations with the SST turbulence model: a) mean velocity profile, b)  $U_+$ -profile, c) turbulent kinetic energy, d)  $\omega$  e)  $v_\tau$  at  $x = 0.97$  and f) skin friction coefficient.

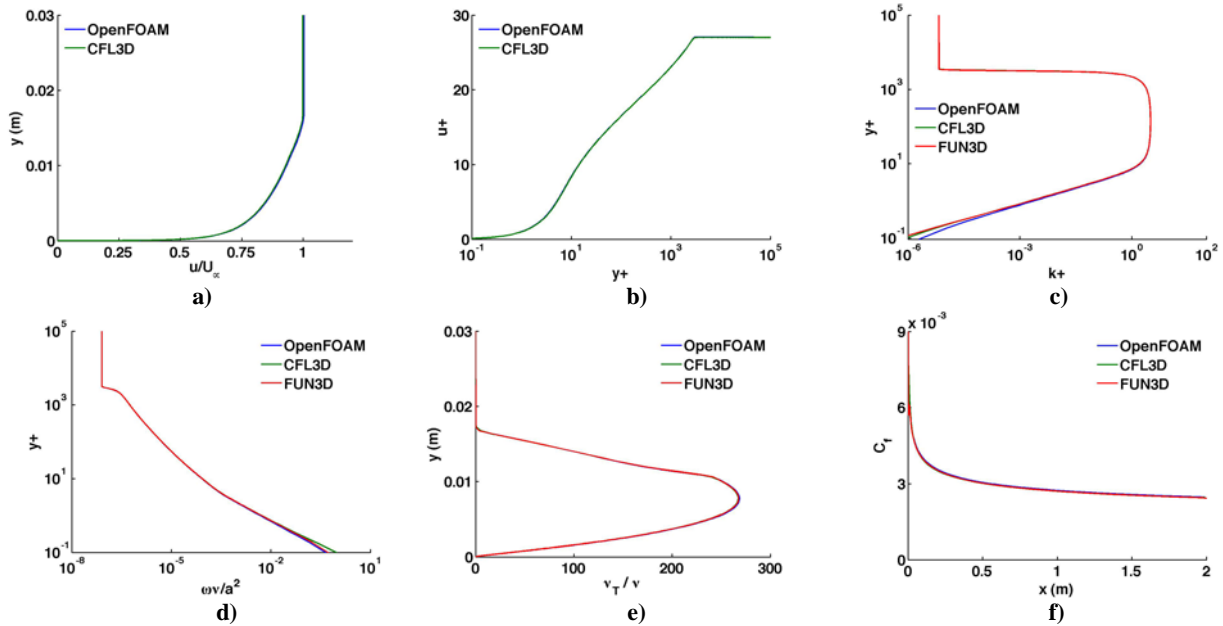


Figure 3. Results of the ZPG flat plate flow simulations with the  $k - \omega$  turbulence model: a) mean velocity profile, b)  $U_+$ -profile, c) turbulent kinetic energy, d)  $\omega$ , e)  $\nu_\tau$  at  $x = 0.97$  and f) skin friction coefficient.

## B. 2-D Bump

Results for a flow over a bump in a channel with the SA, SST, and  $k-\omega$  models are shown in Figs. 4-6. These were obtained on the 705x325 grid. The velocity boundary conditions at the inlet correspond to  $M = 0.2$  and  $Re_L = 3$  million. The turbulent inflow boundary conditions are formulated as they were in a flow over a flat plate. The location  $x = 0.75$  corresponds to the top of the bump. Overall, the three models produce results in good agreement with the NASA data. Some discrepancy is observed for the turbulent viscosity.

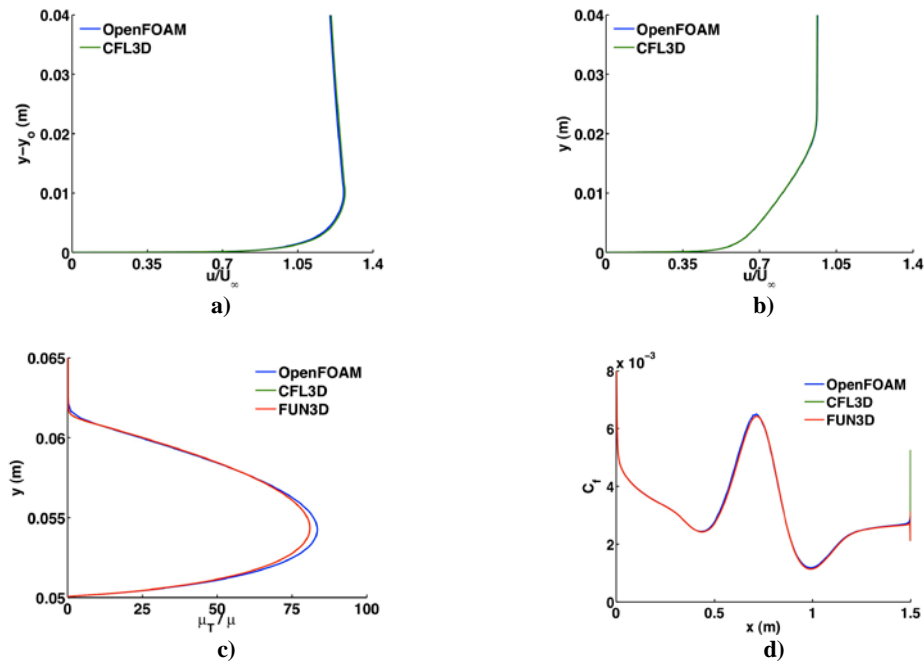


Figure 4. Results of a flow over a 2D bump in a channel with the SA turbulence model: mean velocity profiles at a)  $x = 0.75$  and b)  $x = 1.20148$ , c)  $\nu_\tau$  at  $x = 0.75$ , and d) skin friction coefficient.

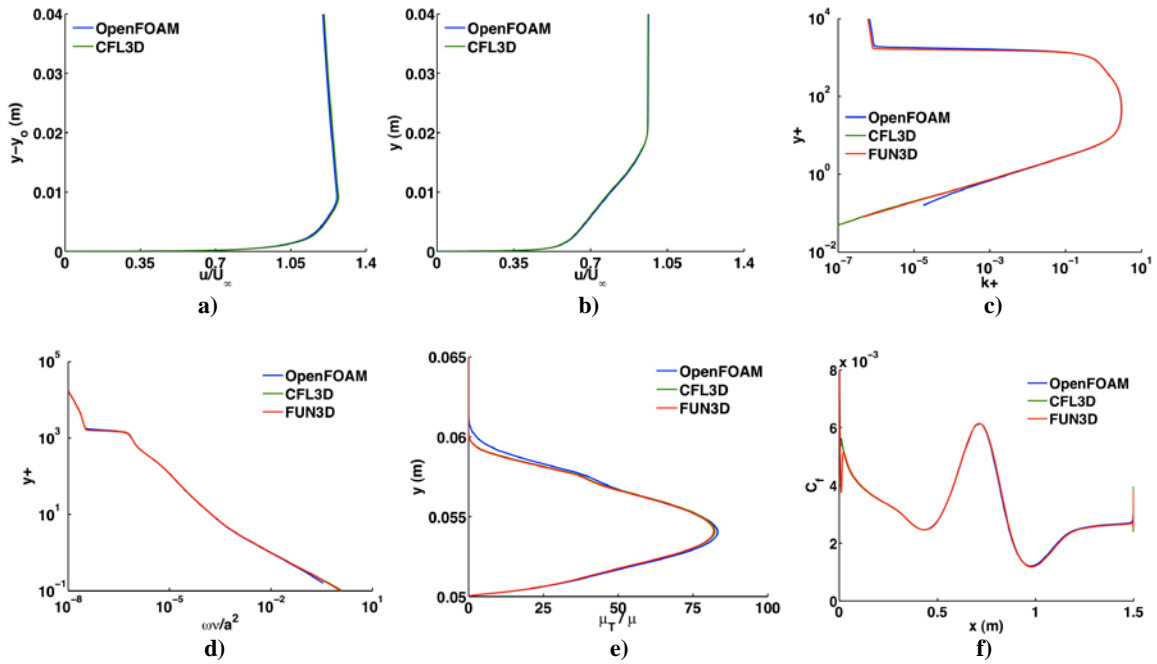


Figure 5. Results of a flow over a 2D bump in a channel with the SST turbulence model: mean velocity profiles at a)  $x = 0.75$  and b)  $x = 1.20148$ , c) turbulent kinetic energy, d)  $\omega$  and e)  $\nu_t$  at  $x = 0.75$  and f) skin friction coefficient.

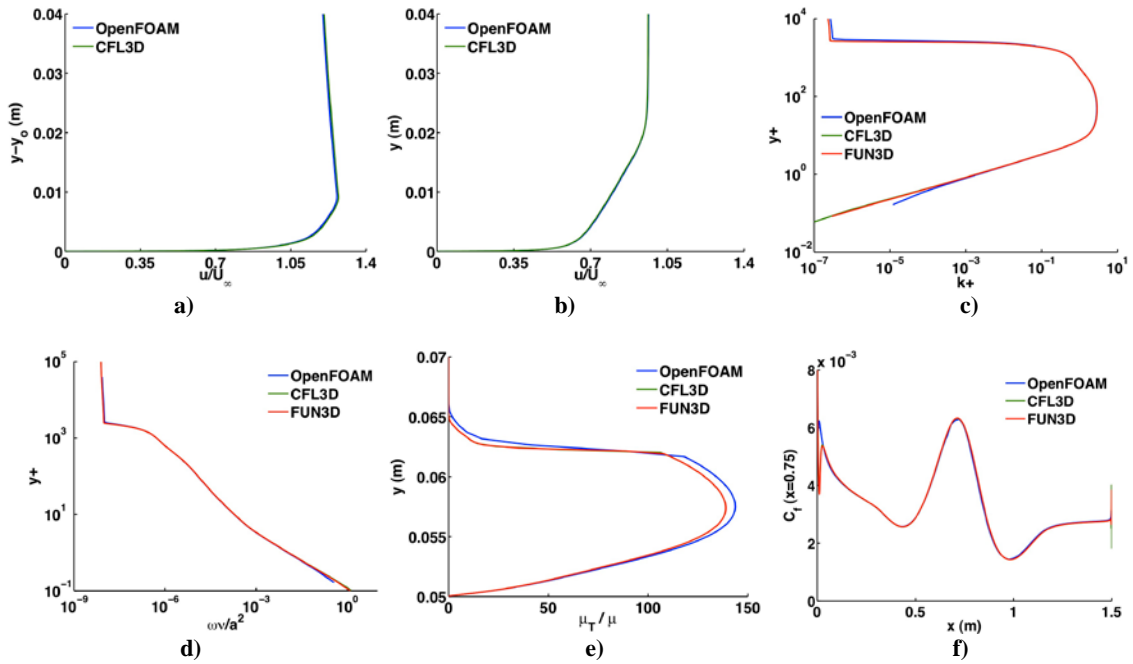


Figure 6. Results of a flow over a 2D bump in a channel with the  $k - \omega$  turbulence model: mean velocity profiles at a)  $x = 0.75$  and b)  $x = 1.20148$ , c) turbulent kinetic energy, d)  $\omega$  and e)  $\nu_t$  at  $x = 0.75$  and f) skin friction coefficient.

### C. Compressibility effects

In the current study, the effect of using compressible vs. incompressible solver in OpenFOAM on the results of simulations was analyzed. Both of NASA's codes are compressible. No substantial compressibility effects on the solutions obtained with OpenFOAM were detected.

### D. Grid convergence analysis

Results of the solution grid convergence study in a flow over a flat plate are shown in Figs. 7 and 8. The OpenFOAM data was obtained with the incompressible solver. In Figure 7, the results obtained with different CFD packages for the skin friction coefficient at  $x = 0.97$  are provided. In the figure, the characteristic mesh length for the constant domain size,  $h$ , is used to analyze the grid resolution effect on the solutions<sup>6</sup>. Figure 8 compares the skin friction profiles obtained with OpenFOAM on different grids.

Similar results for flow over a 2D bump in a channel are shown in Figs. 9-10. The results converge for all solvers. However, the quality of results obtained with OpenFOAM seems to deteriorate on the finest grid, 1409x641. NASA data does not exhibit the same tendency. Multiple tests confirmed that these results are correct for the chosen numerical settings. Thus, the finest grid is not recommended for the use with OpenFOAM in this flow. The coarsest grids are also not recommended for use in both flows with the three models. Notice though that the SA model when implemented in OpenFOAM produces results that are not as sensitive to the grid's variation in a ZPG flow over a flat plate.

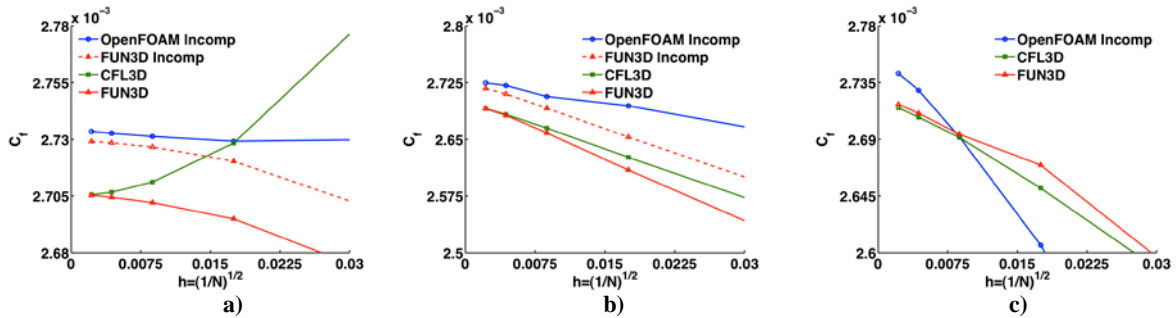


Figure 7. Grid convergence study in a ZPG flat plate flow. Results are obtained with a) SA, b) SST, and c)  $k-\omega$  turbulence models.

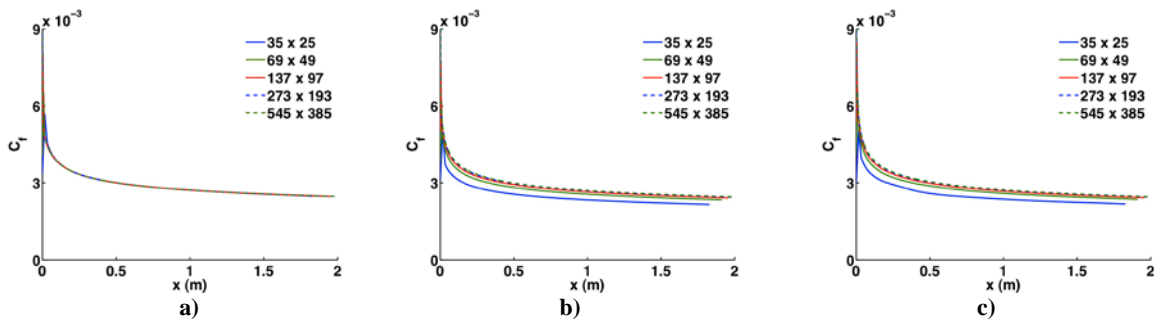


Figure 8. Skin friction coefficient in a ZPG flat plate flow obtained with a) SA, b) SST, and c)  $k-\omega$  turbulence models.

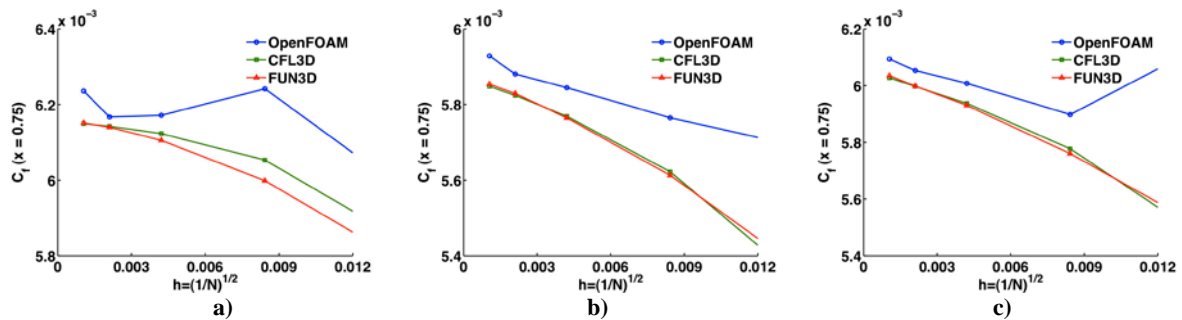


Figure 9. Grid convergence study in a flow over a 2D bump in a channel. Results are obtained with a) SA, b) SST, and c)  $k-\omega$  turbulence models.

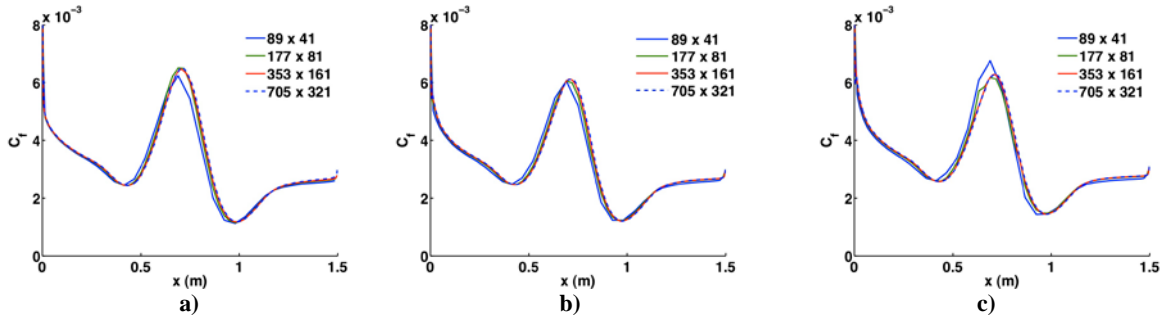


Figure 10. The skin friction coefficient in a flow over a 2D bump in a channel obtained with a) SA, b) SST, and c)  $k-\omega$  turbulence models.

### E. Pressure solvers

The analysis of the pressure solver choice on simulation results was conducted. Solutions obtained with two different linear pressure solvers—generalized geometric-algebraic multi-grid (GAMG) and preconditioned conjugate gradient (PCG)—implemented in OpenFOAM were compared. The number of post sweeps in the GAMG pressure solver was varied from 1 to 4. The pre-conditioners for the PCG pressure solver were diagonal incomplete-Cholesky solver (DIC), faster diagonal incomplete-Cholesky solver (FDIC), and diagonal solver (Diag)<sup>1</sup>.

No difference in computational results was observed due to the pressure solver choice. However, the computational time required for obtaining converged solutions with different solvers varied from one solver to another. CPU time was assessed for simulations on 137x97, 273x193 and 545x385 grids in a ZPG flat plate flow, and on 177x81, 353x161, and 705x321 grids in a flow over a 2D bump in a channel. Computations with each pressure solvers were run for 100,000 iterations. The number of iterations was chosen based on the amount of iterations needed to reach the solution convergence on the finest grid. Tables 1 and 2 compare computational times obtained for each pressure solver with the SA and SST models in the two flows. In a flow over a 2D bump in a channel, the solution convergence could not be obtained with the GAMG linear pressure solver. Therefore, the results for this solver are missing from Table 2.

**Table 1: Computational time required by different pressure solvers in a ZPG flow over a flat plate.**

Flow	Mesh	Pressure Solver	CPU Time (hr:min:sec) SA model	CPU Time (hr:min:sec) SST model
Flat Plate	545 x 385	DIC	58:19:04	70:03:12
		FDIC	69:22:15	67:44:45
		Diagonal	103:34:39	109:22:34
		GAMG (1 post sweeps)	579:16:26	596:14:33
		GAMG (4 post sweeps)	701:13:22	589:37:46
	273 x 193	DIC	22:06:19	23:36:57
		FDIC	22:13:15	23:09:01
		Diagonal	61:33:35	63:09:24
		GAMG (1 post sweeps)	515:46:28	525:34:02
		GAMG (4 post sweeps)	572:31:49	581:54:51
	137 x 97	DIC	5:49:25	6:25:33
		FDIC	5:46:35	6:18:36
		Diagonal	21:03:00	17:09:29
		GAMG (1 post sweeps)	347:03:48	352:08:43
		GAMG (4 post sweeps)	366:23:40	369:32:01

**Table 2: Computational time required by different pressure solvers in a flow over a 2D bump in a channel.**

Flow	Mesh	Pressure Solver	CPU Time (hr:min:sec) SA model	CPU Time (hr:min:sec) SST model
Bump in Channel	705 x 321	DIC	155:38:50	203:35:42
		FDIC	150:03:54	201:04:51
		Diagonal	222:41:28	259:23:50
	353 x 161	DIC	10:28:19	12:28:25
		FDIC	10:34:02	11:58:26
		Diagonal	31:56:36	34:51:43
	177 x 81	DIC	2:34:21	2:23:17
		FDIC	2:09:44	2:21:10
		Diagonal	8:55:37	9:32:43

As the Tables' data shows, the pre-conjugate gradient linear pressure solver with the faster diagonal incomplete-Cholesky preconditioner generates the fastest or closest to the fastest results in all considered cases. Therefore, this is the recommended choice for a pressure solver.

#### F. RST model simulations

Simulations were conducted with the LRR-IP model<sup>5</sup> to test its capability in wall-bounded flows. The model was enhanced with wall corrections<sup>8,9</sup> in models for pressure-strain correlations and dissipation tensor and in the transport equation for the scalar dissipation. Detailed description of the model transport equations can be found in Ref. 7. Results of simulation (not shown here) did not well agree with available experimental and DNS data. More research is necessary to identify sources of observed discrepancies.

#### IV. Acknowledgments

The material is in part based upon work supported by NASA under award NNX12AJ61A. A part of simulations were conducted using the high-performance facilities of the UNM Center for Advanced Research Computing.

#### V. References

- <sup>1</sup>OpenFOAM, Open-source Field Operation and Manipulation, Software Package, Version 2.2.0, 2011, [www.openfoam.com/](http://www.openfoam.com/)
- <sup>2</sup>Spalart, P. R. and Allmaras, S. R., "A One-Equation Turbulence Model for Aerodynamic Flows," *Recherche Aerospaciale*, Vol. 1, 1994, pp. 5-21.
- <sup>3</sup>Wilcox, D. C., "Formulation of the k- $\omega$  Turbulence Model Revisited," *AIAA Journal*, Vol. 46, No.11, 2008.
- <sup>4</sup>Menter, F. R., "Two-Equation Eddy-Viscosity Turbulence Models for Engineering Applications," *AIAA Journal*, Vol. 32, No.8, August 1994, pp. 1598-1605.
- <sup>5</sup>Launder, B. E., Reece, G. J., Rodi, W., "Progress in the development of a Reynolds Stress turbulence closure," *J. Fluid Mech.*, Vol. 68, 1975, pp.537-566.
- <sup>6</sup>Turbulence Model Benchmarking Working Group Turbulence Modeling Resource, NASA Langley, <http://turbmodels.larc.nasa.gov/>
- <sup>7</sup>Kurbatskii, A. F., Poroseva, S. V., "Modeling turbulent diffusion in a rotating cylindrical pipe flow", *Int. J. Heat and Fluid Flow*, 1999, Vol. 20, No. 3, pp. 341-348.
- <sup>8</sup>So, R. M. C., Yoo, G. J., "Low Reynolds Number Modeling of Turbulent Flows With and Without Wall Transpiration", *AIAA Journal*, 1987, Vol. 25, No. 12, pp.1556-1564.
- <sup>9</sup>Gibson, M. M., Launder, B. E., "Ground effects on pressure fluctuations in the atmospheric boundary layer," *J. Fluid Mech.*, Vol. 86, 1978, pp. 491-511.